Neutral stability curves of low-frequency Görtler flow generated by free-stream vortical disturbances

Samuele Viaro[1]† and Pierre Ricco[1]

[1]Department of Mechanical Engineering, The University of Sheffield, Sheffield, S1 3JD, UK

(Received xx; revised xx; accepted xx)

The neutral curves of the boundary-layer Görtler-vortex flow generated by free-stream disturbances, i.e., curves that distinguish the perturbation flow conditions of growth and decay, are computed through a receptivity study for different Görtler numbers, wavelengths, and low frequencies of the free-stream disturbance. The perturbations are defined as Klebanoff modes or strong and weak Görtler vortices, depending on their growth rate. The critical Görtler number below which the inviscid instability due to the curvature never occurs is obtained and the conditions for which only Klebanoff modes exist are thus revealed. A streamwise-dependent receptivity coefficient is defined and we discuss the impact of the receptivity on the N-factor approach for transition prediction.

Key words: boundary layer stability, boundary layer receptivity, Görtler vortices

1. Introduction

In 1940, Görtler (1940) discovered a flow instability in the form of counter-rotating longitudinal vortices caused in boundary layers over concave surfaces by an imbalance between pressure and centrifugal forces. These perturbations have thereafter been called Görtler vortices. Hall (1983, 1990) identified the key features for the rigorous theoretical description of the Görtler vortices. The full Navier-Stokes equations can be simplified to the parabolic three dimensional boundary-layer equations in the limit of large Reynolds numbers, where the effect of curvature is distilled in the Görtler number, i.e., the ratio between the squared Reynolds number and the dimensionless radius of curvature, appearing in a convection term of the wall-normal momentum equation. The mathematical consequence of the parabolic character of the system is that, to describe the flow correctly, these equations must be complemented by rigorous initial conditions (near the leading edge) and outer boundary conditions (free-stream and wall), i.e., the receptivity to external disturbances must be included in the formulation. Hall (1982) thus proved that an eigenvalue formulation, for example following from the parallel-flow assumption and leading to a system of ordinary differential equations, is only valid as an asymptotic approximation for the study of Görtler flows in the limits of large Görtler number and short spanwise wavelength. Hall (1983) also showed the strong dependence of the solution on the initial conditions, thereby confirming that a unique neutral curve does not exist if the initial conditions vary.

The correct mathematical description of the influence of low-frequency free-stream

† Email address for correspondence: sviaro1@sheffield.ac.uk

disturbances on flat plate boundary layers, which translates into the unequivocal form of the initial and free-stream boundary conditions, was formulated by Leib *et al.* (1999). Their theory focuses on the dynamics of streamwise elongated perturbations inside the boundary layer, widely recognized as the cause of bypass transition, i.e., the route to turbulence where Tollmien-Schlichting (TS) waves do not play a significant role. These boundary-layer perturbations take the form of streaky structures and are often called Klebanoff modes. Wu *et al.* (2011) extended the flat-plate theory of Leib *et al.* to study the linear evolution of incompressible Görtler vortices subject to free-stream vortical disturbances which, in their initial linear stage, resemble Klebanoff modes. Thanks to these theoretical advancements, the Görtler flow is precisely and uniquely linked to the characteristics of the free-stream disturbances. The issue of the strong dependence of the Görtler vortices on the arbitrary initial conditions shown by Hall (1983) has therefore been resolved for flows exposed to free-stream disturbances, while the receptivity to wall roughness has been studied by Bassom & Seddougui (1995) and by Sescu & Thompson (2015). However, Görtler-flow neutral curves, i.e., curves in the parameter space which separate regions of growth and decay of the boundary-layer perturbations, were not computed by Wu *et al.* (2011) and it thus remains an open problem. This is in contrast to the search for the neutral curve of the TS waves, which was solved by Tollmien (1929).

We use the receptivity-stability framework developed by Wu *et al.* (2011) to achieve three objectives. First we compute the neutral curves for different Görtler numbers and characteristics of the free-stream disturbance, for both Klebanoff modes and Görtler vortices. These neutral curves define the regions of stability from the leading edge for the entire range of the spanwise wavenumber and low frequency. The flat plate scenario is included in the analysis. The neutral curves also identify the minimum Görtler number below which the perturbation does not develop into Görtler vortices even in the presence of curved surfaces and the maximum Görtler number above which Klebanoff modes, which are always present near the leading edge, evolve directly into Görtler vortices. The study of the neutral curve is also relevant because it finds the conditions for which the Görtler instability affects the wall-shear stress significantly. Extending the receptivity analysis of Wu *et al.*, we propose a modified receptivity coefficient which allows us to obtain the maximum amplitude of the boundary-layer perturbations from the local eigenvalue solution. Finally, we discuss the use of the N-factor approach, widely used by engineers for the prediction of transition to turbulence (Van Ingen 1956; Jaffe *et al.* 1970), when the receptivity of the boundary layer to free-stream disturbances is included in the formulation.

2. Mathematical framework

2.1. *Flow definition and scaling*

We consider an incompressible uniform flow of velocity U_∞^* past a concave plate with constant radius of curvature r^*. The flow is shown in figure 1 and hereinafter the asterisk * identifies dimensional quantities. A boundary layer forms over the curved plate. Free-stream vortical disturbances are passively advected by the uniform free-stream flow and are modelled as three-dimensional vortical disturbances of the gust type, which, sufficiently upstream and away from the plate, have the form

$$\mathbf{u} - \mathbf{i} = \epsilon \hat{\mathbf{u}}^\infty \, e^{i\left(\mathbf{k}\cdot\mathbf{x} - k_x \mathrm{R}\hat{t}\right)} + \text{c.c.}, \tag{2.1}$$

where ϵ is a small parameter, $\mathbf{x} = \{x, y, z\}$ denotes the streamwise, wall-normal, and spanwise directions, $\mathbf{k} = \{k_x, k_y, k_z\}$ defines the wavenumber vector, $\hat{\mathbf{u}}^\infty = \{\hat{u}^\infty, \hat{v}^\infty, \hat{w}^\infty\}$

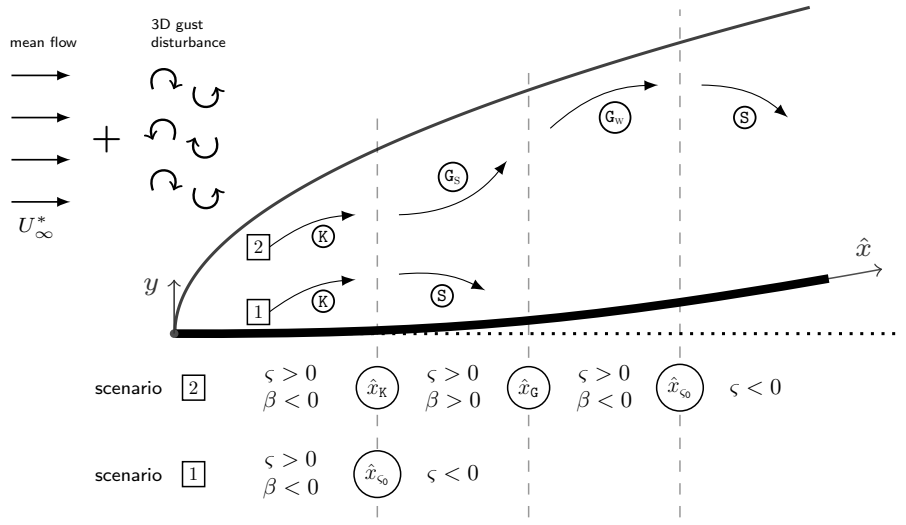

Figure 1: Schematic of growth and decay of boundary-layer perturbations based on the parameters ς and β defined in (2.3). The sketch represents K-vortices (K), Görtler vortices with strong growth ($\mathtt{G}_\mathrm{S}$), Görtler vortices with weak growth ($\mathtt{G}_\mathrm{W}$), and stable flows (S). In the steady case, scenario 1 is typical for $\mathtt{G} < \mathtt{G}_\mathrm{B} = 10.9$, while scenario 2 is typical for $\mathtt{G} > \mathtt{G}_\mathrm{C} = 17$.

is the amplitude of the free-stream disturbance, c.c. indicates the complex conjugate, and $\mathbf{i}$ is the unit vector of the streamwise direction. The wavenumber vector $\mathbf{k}$ and the velocity vector $\hat{\mathbf{u}}^\infty$ satisfy the solenoidal condition $\mathbf{k} \cdot \hat{\mathbf{u}}^\infty = 0$. Lengths are scaled by $\Lambda_z^* = \lambda_z^*/2\pi$, where λ_z^* is the spanwise wavelength of the gust, velocities are scaled by U_∞^*, and the pressure is scaled by $\rho^* {U_\infty^*}^2$, where ρ^* is the density of the fluid. We define the Reynolds number $\mathtt{R} = U_\infty^* \Lambda_z^*/\nu^* \gg 1$, where ν^* is the kinematic viscosity of the fluid, and the Görtler number $\mathtt{G} = \mathtt{R}^2 \Lambda_z^*/r^* = O(1)$. The dimensionless spanwise wavenumber is $k_z = 1$ and the frequency parameter is $k_x\mathtt{R}$. Since the interest is in streamwise elongated perturbations, the streamwise coordinate and time are scaled as $\hat{x} = x^*/(\mathtt{R}\Lambda_z^*)$ and $\hat{t} = U_\infty^* t^*/(\mathtt{R}\Lambda_z^*)$, respectively. The boundary-layer velocity and pressure $\mathbf{q}(\mathbf{x}, t) = \{u, v, w, p\}(\mathbf{x}, t)$ are decomposed into their mean $\mathbf{Q}(\mathbf{x})$ and perturbation $\mathbf{q}'(\mathbf{x}, t)$ as $\mathbf{q} = \mathbf{Q} + \epsilon\mathbf{q}'$. The mean flow is the Blasius boundary layer and the perturbations are

$$\mathbf{q}' = ik_z\breve{w} \left\{ \mathtt{R}\bar{u},\ (2\hat{x})^{1/2}\bar{v},\ \frac{1}{ik_z}\bar{w},\ \frac{1}{\mathtt{R}}\bar{p} \right\} e^{i\left(k_z z - k_x \mathtt{R}\hat{t}\right)} + \text{c.c.}, \tag{2.2}$$

where $\breve{w} \equiv \hat{w}^\infty + ik_z\hat{v}^\infty/(k_x^2 + k_z^2)^{1/2} = O(1)$ and only the three-dimensional part of the perturbation has been considered (Leib *et al.* 1999). In the limits of large Reynolds number $\mathtt{R} \gg 1$, small perturbations $\epsilon \ll 1/\mathtt{R}$, and low frequency $k_x \ll 1$, the linearized unsteady boundary region (LUBR) equations for the perturbation flow are recovered by inserting the flow decomposition, along with (2.2), into the full Navier-Stokes and continuity equations and collecting $O(\epsilon)$ terms. Details of the mathematical methodology are found in Leib *et al.* (1999) and Wu *et al.* (2011). The LUBR equations are parabolic along the streamwise direction and are coupled with initial and boundary conditions derived through asymptotic matching with the oncoming free-stream vortical disturbances (Leib *et al.* 1999; Wu *et al.* 2011). A second-order implicit finite-difference scheme has been

used to solve the LUBR equations (Ricco & Wu 2007). The three parameters influencing the flow are $\mathtt{G}$, k_y and $k_x\mathtt{R}$. They account for the effects of curvature, ratio of the free-stream spanwise wavelength to the wall-normal wavelength, and frequency, respectively. To stress the importance of receptivity, we note that the solution is influenced by k_y only through the initial and boundary conditions as k_y does not appear in the LUBR equations (Leib *et al.* 1999; Wu *et al.* 2011).

2.2. *Neutral curve parameters*

In previous representations of Görtler-flow neutral curves (Hall 1990), the spanwise wavenumber, scaled by the boundary-layer thickness, often appeared on the abscissa and a scaled Görtler number on the ordinate. In our scaling, this would translate into an $\mathcal{X}$-$\mathcal{G}$ plane, where $\mathcal{X} = (2\hat{x})^{1/2}$ and $\mathcal{G} = \mathtt{G}\mathcal{X}^3/\sqrt{2}$, causing the neutral curve to collapse on a $\mathcal{X}^3$ curve, without fully revealing the flow behavior, especially near the leading edge. We instead choose to represent the neutral curve in the $\hat{x}$-$\mathtt{G}$ plane so that for moderate $\mathtt{G}$ the presence of Klebanoff modes and Görtler vortices is linked more distinctly with the flow stability. The neutral curves are thus found for different values of $k_x\mathtt{R}$ and k_y in the $\hat{x}$-$\mathtt{G}$ plane.

The neutral curves are represented by the parameters

$$\varsigma(\hat{x}) \equiv \frac{\mathrm{d}\mathtt{E}(\hat{x})}{\mathrm{d}\hat{x}}, \qquad\qquad \beta(\hat{x}) \equiv \frac{\mathrm{d}^2|\bar{u}(\hat{x})|_{\max}}{\mathrm{d}\hat{x}^2}, \tag{2.3}$$

where $\mathtt{E}(\hat{x}) \equiv \int_0^\infty |\bar{u}(\hat{x},\eta)|^2 \mathrm{d}\eta$ is the scaled perturbation energy divided by $(2\hat{x})^{1/2}$ (Hall 1990) and $|\bar{u}(\hat{x})|_{\max} \equiv \max_\eta |\bar{u}(\hat{x},\eta)|$ is the maximum along $\eta = y/(2\hat{x})^{1/2}$ of the amplitude of the streamwise velocity perturbation. This definition of $\varsigma(\hat{x})$ is well suited for the receptivity analysis since it retains the information from the perturbation amplitude. The latter would not enter the picture if the $\hat{x}$-derivative of the energy were normalized by the energy itself, as in Hall (1990). Only the $|\bar{u}|$ component is used to define the scaled perturbation energy in (2.3) because the physical streamwise velocity component for the Görtler vortices is much larger than the transverse velocity components (Wu *et al.* 2011).

Figure 1 summarizes how the instabilities are categorized according to (2.3). The flow is unstable for $\varsigma > 0$ and stable for $\varsigma < 0$, with $\varsigma = 0$ defining the neutral points located at $\hat{x} = \hat{x}_{\varsigma_0}$. Since curvature effects are not at work near the leading edge, the boundary-layer perturbations start growing from the leading edge as Klebanoff modes, herein labelled $\mathtt{K}$-vortices (K), for which $\varsigma > 0$, $\beta < 0$. Depending on $\mathtt{G}$, $k_x\mathtt{R}$ and k_y, $\mathtt{K}$-vortices can either become stable downstream of $\hat{x} = \hat{x}_{\varsigma_0}$ or turn into Görtler vortices at $\hat{x} = \hat{x}_{\mathtt{K}}$, where $\beta = 0$ and $\beta'(\hat{x}) > 0$, with the prime indicating the derivative with respect to $\hat{x}$. The Görtler vortices are characterized by an initial strong growth, denoted by ($\mathtt{G}_\mathrm{S}$), for which $\beta > 0$ ($\mathtt{G}_\mathrm{S}$-vortices). When $\beta = 0$ and $\beta' < 0$ at $\hat{x} = \hat{x}_{\mathtt{G}}$, the local growth rate is maximum and downstream their growth weakens as $\beta < 0$ ($\mathtt{G}_\mathrm{W}$-vortices, ($\mathtt{G}_\mathrm{W}$)), until they eventually stabilize downstream of $\hat{x} = \hat{x}_{\varsigma_0}$.

3. Results

3.1. *Downstream evolution of the disturbance energy*

The scaled perturbation energy $\mathtt{E}(\hat{x})$ of both $\mathtt{K}$-vortices and Görtler vortices, normalized by the maximum value $\mathtt{E}_{\max,\mathtt{G}_0} \equiv \max_{\hat{x}} |\mathtt{E}(\hat{x})|_{\mathtt{G}=0}$ for $\mathtt{G} = 0$, is shown in figure 2 as a function of $\hat{x}$ for $k_x\mathtt{R} = 0$ and $k_y = 2$. Energy maxima, $\mathtt{M}_1$ and $\mathtt{M}_2$, and minima $\mathtt{m}$ identify stable conditions, i.e., where $\varsigma = 0$. Three critical Görtler numbers occur for this configuration,

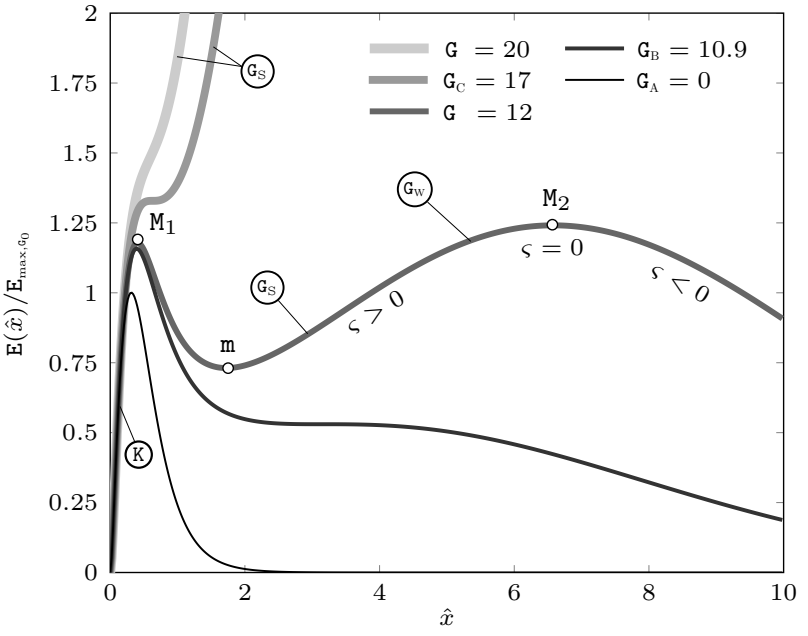

Figure 2: Perturbation energy $\mathtt{E}(\hat{x})$ normalized by $\mathtt{E}_{\mathrm{max},\mathtt{G}_0}$, the maximum value of $\mathtt{E}$ for $\mathtt{G} = 0$, as a function of $\hat{x}$ for $k_x\mathtt{R} = 0$ and $k_y = 2$.

i.e., $\mathtt{G}_\mathrm{A}$, $\mathtt{G}_\mathrm{B}$, and $\mathtt{G}_\mathrm{C}$. In the flat-plate case, for which $\mathtt{G} = \mathtt{G}_\mathrm{A} = 0$, only K-vortices are present. They start growing from the leading edge and then dissipate rapidly due to viscosity (Leib *et al.* 1999) as in scenario 1 of figure 1. As the curvature is introduced, the imbalance between pressure and centrifugal forces energizes the boundary-layer perturbation. Only for $\mathtt{G} > \mathtt{G}_\mathrm{B} = 10.9$ the Görtler vortices become unstable as secondary growing disturbances after the viscous decay of the K-vortices. A new maximum $\mathtt{M}_2$ thus emerges. Following the evolution of the perturbation for $\mathtt{G} = 12$, figure 2 shows that K-vortices represent the initial instability of the boundary layer, which start stabilizing at $\mathtt{M}_1$. After the viscous decay, the onset of the Görtler vortices causes the boundary layer to become unstable again at m. Their initial strong growth (G$_\mathrm{S}$) shifts into a weak growth (G$_\mathrm{W}$) at $\hat{x} = \hat{x}_\mathtt{G}$ before ultimately stabilizing again at $\mathtt{M}_2$. In the range $\mathtt{G}_\mathrm{B} < \mathtt{G} < \mathtt{G}_\mathrm{C} = 17$ both instabilities are thus present. Figure 2 also shows that for $\mathtt{G} > \mathtt{G}_\mathrm{C}$ the K-vortices turn into Görtler vortices directly without the intermediate viscous decay: the first peak $\mathtt{M}_1$ in the scaled energy distribution is not present anymore and the perturbation thus evolves as in scenario 2 in figure 1.

3.2. *Neutral curves*

We can now obtain a neutral stability curve in the $\hat{x}$-G plane for each pair of parameters $(k_x\mathtt{R},\, k_y)$.

3.2.1. *Steady Görtler-flow scenario*

The neutral curve for $k_x\mathtt{R} = 0$ and $k_y = 2$ is shown in figure 3. The continuous black line represents the neutral curve, the black dotted line indicates the streamwise location $\hat{x}_\mathtt{K}$ where K-vortices turn into Görtler vortices directly, and the black dashed line represents the streamwise location $\hat{x}_\mathtt{G}$ where the growth of the Görtler vortices shifts from strong to weak. Three critical points of the neutral curve, A, B, C, are shown in figure 3. Point A

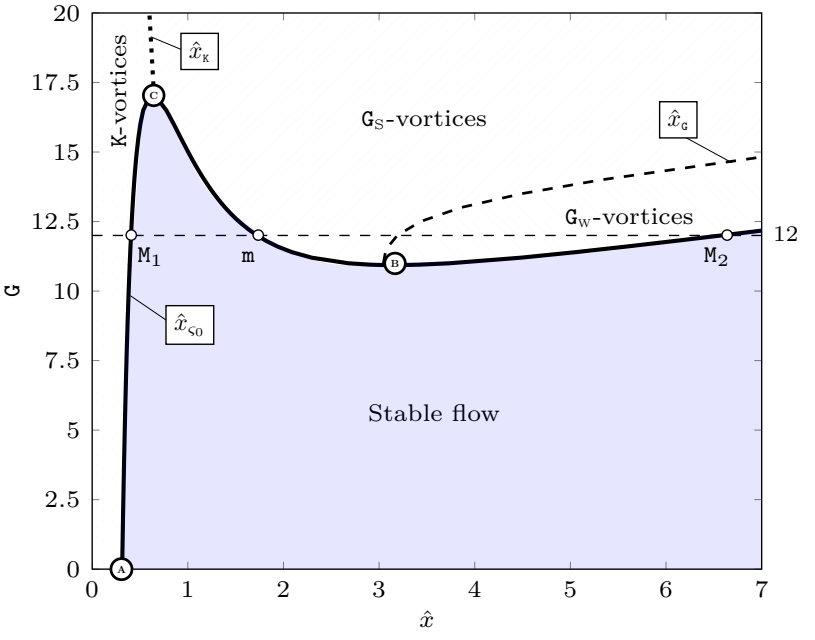

Figure 3: Neutral stability curve, $\hat{x} = \hat{x}_{\varsigma_0}$ (▬), and curves at which the K-vortices turn into $\mathtt{G}_{\mathrm{S}}$-vortices, $\hat{x} = \hat{x}_{\mathrm{K}}$ (▪▪▪), and the $\mathtt{G}_{\mathrm{S}}$-vortices turn into $\mathtt{G}_{\mathrm{W}}$-vortices, $\hat{x} = \hat{x}_{\mathtt{G}}$ (▬ ▬ ▬), for $k_x\mathtt{R} = 0$, $k_y = 2$.

indicates the $\hat{x}$ location downstream of which the K-vortices are stable for $\mathtt{G} = 0$, while point B denotes the $\hat{x}$ location of the local minimum of the neutral curve, corresponding to the Görtler number ($\mathtt{G}_{\mathrm{B}} = 10.9$) below which only K-vortices exist. Point C indicates the $\hat{x}$ location of the local maximum of the neutral curve corresponding to the Görtler number ($\mathtt{G}_{\mathrm{C}} = 17$) above which K-vortices shift directly to Görtler vortices.

The neutral curve shows that K-vortices always exist near the leading edge for any Görtler number and that increasing the Görtler number strengthens the inviscid nature of the Görtler instability, thereby causing the unstable region to expand rapidly. As the curvature increases, the point m, also shown in figure 2, moves closer to the leading edge and eventually merges with $\mathtt{M}_1$ for $\mathtt{G} = \mathtt{G}_{\mathrm{C}}$. For $\mathtt{G} > \mathtt{G}_{\mathrm{C}}$, the boundary layer is unstable from the leading edge as K-vortices turn into Görtler vortices at $\hat{x} = \hat{x}_{\mathrm{K}}$. If the perturbation energy were defined by integrating $|\bar{u}|$ over y for the definition of ς, the neutral curve would be slightly shifted to lower G but would retain its shape.

In the limit $\mathtt{G} \gg 1$, the asymptotic analysis of Wu *et al.* (2011) shows that the perturbation undergoes two pre-modal stages before it exhibits exponential growth. The K-vortices experience a first change in their dynamics when $\hat{x}_{\mathrm{I}} = O\left(\mathtt{G}^{-2/3}\right)$, i.e., when curvature effects start influencing the pressure field which, at this stage, is decoupled from the velocity field. Further downstream, the second pre-modal stage ensues when $\hat{x}_{\mathrm{II}} = O\left(\mathtt{G}^{-2/5}\right)$, i.e., when the wall-normal gradient of the pressure perturbations becomes comparable with the convection terms, thus defining the onset of the Görtler instability. Figure 4 depicts the extension of figure 3 for large G numbers at small $\hat{x}$. The red dashdotted lines in figure 4 indicate the large-G pre-modal asymptotic limits, clearly showing that $\hat{x}_{\mathrm{I}} < \hat{x}_{\mathrm{K}} < \hat{x}_{\mathrm{II}}$ as G increases. This confirms that β is appropriate for assessing the location where K-vortices turn into Görtler vortices and our approach

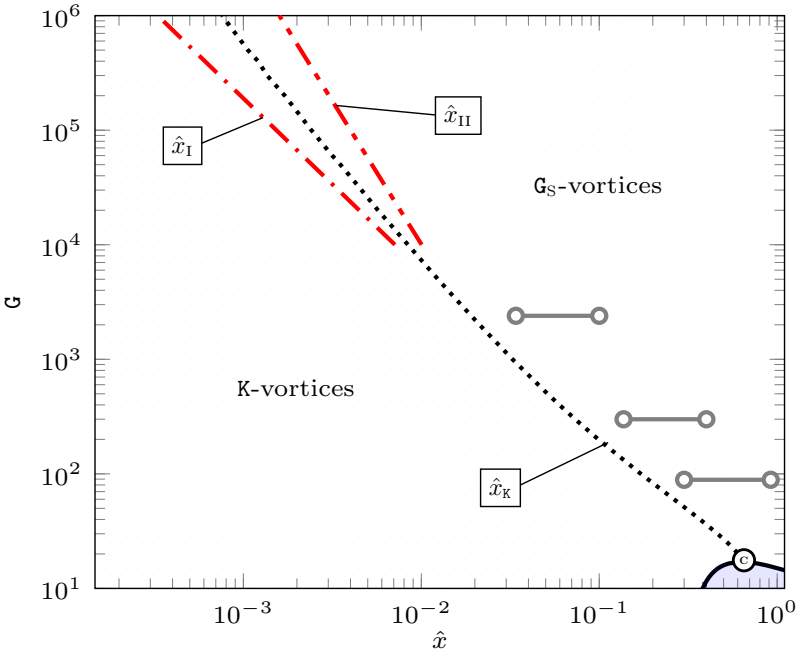

Figure 4: Curve at which the K-vortices turn into $\mathtt{G}_{\rm S}$-vortices, $\hat{x} = \hat{x}_{\rm K}$ (▪▪▪), and neutral stability curve, $\hat{x} = \hat{x}_{\varsigma_0}$ (▬), for $k_x\mathtt{R} = 0$, $k_y = 2$, and large G numbers. The experimental values by Boiko *et al.* (2010) (○——○) and the asymptotic limits by Wu *et al.* (2011) for $\mathtt{G} \gg 1$, $\hat{x}_{\rm I} = O\left(\mathtt{G}^{-2/3}\right)$ (▬·▬) and $\hat{x}_{\rm II} = O\left(\mathtt{G}^{-2/5}\right)$ (▬·▪·▬), are shown.

λ_z^*	x_A^*	r_A^*	x_B^*	r_B^*	x_C^*	r_C^*
0.002	0.02	∞	0.04	0.68	0.19	1.06
0.004	0.08	∞	0.15	5.46	0.78	8.51
0.008	0.31	∞	0.61	43.68	3.01	68.06

Table 1: Physical locations in meters of the critical stability points for $k_x\mathtt{R} = 0$ and $k_y = 2$, estimated from the experimental work by Boiko *et al.* (2010).

is consistent with the large-G analysis of Wu *et al.* (2011). In particular, we find that $\hat{x}_{\rm K} = O\left(\mathtt{G}^{-0.52}\right)$ in the range $10^4 < \mathtt{G} < 10^6$.

It is also important to set experimental results of Görtler vortices within our theoretical framework. Görtler vortices induced by free-stream disturbances over concave surfaces were experimentally studied by Boiko *et al.* (2010) for a wide range of parameters: $r^* = 8.37$ m, $\lambda_z^* = 0.008, 0.012, 0.024$, and unit Reynolds number $\mathtt{R}_{\rm U}^* = U_\infty^*/\nu^* = 6{\cdot}10^5$ m^{-1}. As expected, in their $\hat{x}$-range of investigation, the Görtler instability is within the unstable $\mathtt{G}_{\rm S}$-vortex region of figure 4. The dimensional values summarized in table 1 demonstrate that the three critical points of the neutral curve could be studied experimentally by adjusting the radius of curvature and the characteristics of the free-stream disturbance.

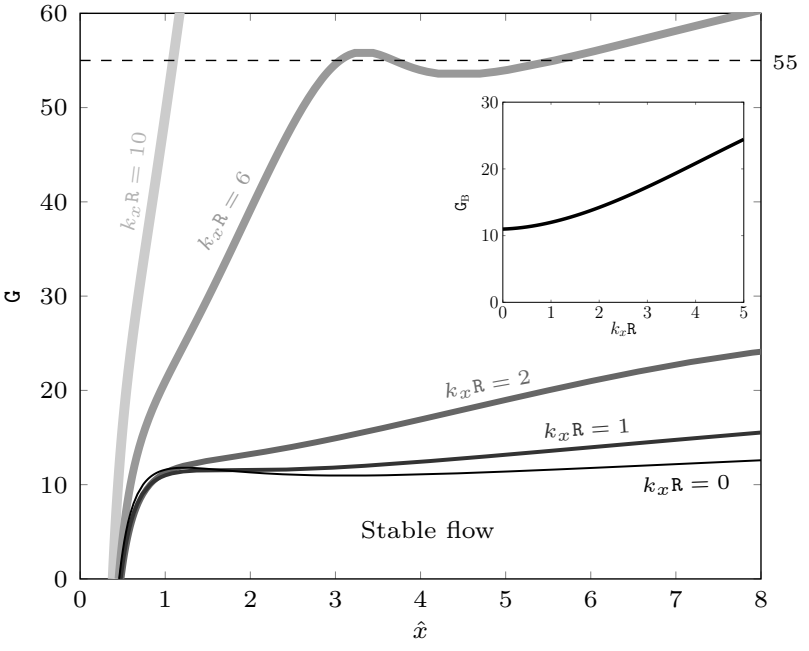

Figure 5: Neutral stability curves $\varsigma = 0$ for $k_y = 1$ and different values of the frequency $k_x\mathtt{R}$. Inset: variation of the critical Görtler number $\mathtt{G}_\mathtt{B}$ as a function of $k_x\mathtt{R}$ for $k_y = 1$.

3.2.2. *Effect of frequency and wavelength ratio*

Figures 5 and 6 show the influence of the frequency parameter $k_x\mathtt{R} = \mathtt{R}\lambda_z^*/\lambda_x^*$ and the wavelength ratio $k_y = \lambda_z^*/\lambda_y^*$, respectively, on the neutral stability curves. For all cases, the $\hat{x}_\mathtt{K}$ lines overlap for most Görtler numbers (not shown) and, sufficiently downstream, the neutral curves become independent of the initial conditions that are herein linked to the free-stream disturbances. Figure 5 shows that the stability region expands significantly as the frequency increases for free-stream disturbances with equal transverse wavelengths λ_z^* and λ_y^* ($k_y = 1$). Boundary-layer perturbations generated by steady free-stream disturbances are therefore the most likely to turn into Görtler vortices through inviscid instability. When $k_x\mathtt{R} > 2$, there is a range of Görtler numbers for which the boundary layer becomes unstable again after an initial decay of Görtler vortices and before entering the permanent stable region. This scenario is shown in figure 5 for $k_x\mathtt{R} = 6$ and $\mathtt{G} = 55$. For higher frequencies, this phenomenon is even more accentuated as it occurs for a larger range of Görtler numbers. However, we focus on low-frequency disturbances as these are the most unstable and are fully consistent with our asymptotic framework, which is based on $k_x \ll 1$.

It is also important to estimate whether TS waves may be excited by leading-edge receptivity mechanisms over flat plates (Goldstein 1983; Ricco & Wu 2007) in the low-frequency scenario proper of the neutral curves studied herein. For the laboratory conditions of Boiko *et al.* (2010) and the flat-plate case, via an in-house spatial stability code (Ricco 2009) we computed the neutral locations $\hat{x}$ downstream of which three-dimensional time-periodic TS waves grow spatially. It is sufficient to study the case at the highest frequency, $k_x\mathtt{R} = 10$, because the neutral stability point moves downstream as the frequency decreases. By employing the Squire transformation (Squire 1933), which is valid for neutral conditions in the spatial stability case, we find that for our characteristic

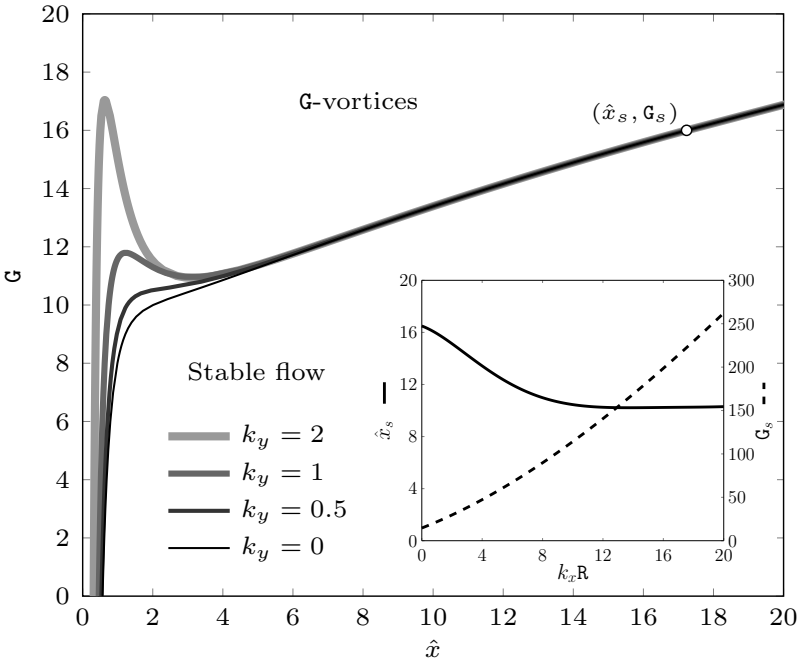

Figure 6: Neutral stability curves $\varsigma = 0$ for different values of the wall-normal wavenumber k_y and $k_x\mathtt{R} = 0$. Inset: streamwise location $\hat{x}_s$ where the neutral curve becomes independent on k_y and the corresponding Görtler number $\mathtt{G}_s$ for different frequencies $k_x\mathtt{R}$.

spanwise wavenumbers, $2\pi\delta^*/\lambda_z^* \approx 2.5$, where δ^* is the displacement thickness, three-dimensional TS waves are always stable. Three-dimensional TS waves would start growing only for $2\pi\delta^*/\lambda_z^*$ smaller than about 0.08, which corresponds to very large spanwise wavelengths, i.e., larger than about 0.4m.

At higher frequencies, the TS waves start amplifying at smaller $\hat{x}$, but $k_x\mathtt{R}$ becomes too large and therefore our assumptions of low frequency and streamwise-elongated perturbations do not hold. The streamwise pressure gradient and the streamwise viscous effects of the perturbations come into play and the full linearized Navier-Stokes equations must be solved or some other asymptotic formalism, such as triple-deck theory, must be adopted. Boiko *et al.* (2010) indeed included these streamwise effects in their equations and computed the TS waves, but did not account for the receptivity to external disturbances, a key ingredient in the analysis of Wu *et al.* (2011) and in our study.

The inset of figure 5 shows the increase of the critical Görtler number $\mathtt{G}_\mathrm{B}$ with $k_x\mathtt{R}$. Results for different k_y are not shown as they overlap on the same curve due to $\mathtt{G}_\mathrm{B}$ being near the location where the neutral curves are independent of k_y.

Figure 6 shows the influence of the wall-normal wavenumber k_y for $k_x\mathtt{R} = 0$. The most critical scenario is for $k_y = 0$. As k_y increases, i.e., as λ_z^* becomes progressively larger than λ_y^*, stability increases near the leading edge for both steady and unsteady flows, whereas the neutral curve becomes independent of k_y downstream of a location $\hat{x}_s$, defined as the $\hat{x}$ location where the neutral points at different k_y remain within a range $\Delta\hat{x} < 0.0005$. This is in agreement with the results of Hall (1990) at large $\hat{x}$ locations. The streamwise location $\hat{x}_s$ is shown as a function of $k_x\mathtt{R}$ in the inset of figure 6. As the frequency increases, $\hat{x}_s$ decreases and it becomes nearly independent of the frequency

for $k_x\mathtt{R} > 10$. The Görtler number $\mathtt{G}_s$ associated with $\hat{x}_s$ increases monotonically with $k_x\mathtt{R}$. Based on the experimental conditions of Boiko *et al.* (2010), $\hat{x}_s = 10$ corresponds to $x^* \approx 22$m, which means that the independence of the neutral curves on k_y is not reached in realistic scenarios. As k_y only occurs in the free-stream boundary conditions at leading order, this further confirms the crucial importance of solving the receptivity problem, i.e., of precisely specifying the free-stream disturbance, for the correct description of the Görtler-flow dynamics.

3.3. *Receptivity coefficient*

It is of practical interest to investigate the role that the outer disturbances play on the boundary-layer perturbations through a receptivity coefficient $\mathtt{A}$, defined as follows. Following (3.1) of Wu *et al.* (2011), we first introduce the eigenvalue solution (EV) in the form

$$\bar{u}_e(\hat{x},\eta) = \widetilde{u}_e(\eta)\; e^{\int_{\hat{x}_\mathrm{M}}^{\hat{x}} \sigma_{\mathrm{EV,\,Re}}(x)\mathrm{d}x}, \tag{3.1}$$

where $\sigma_{\mathrm{EV}}(\hat{x})$ is a complex number whose real part $\sigma_{\mathrm{EV,\,Re}}(\hat{x}) \equiv \Re\{\sigma_{\mathrm{EV}}(\hat{x})\}$ is the local growth rate and $\hat{x}_\mathrm{M}$ is a streamwise location where the solution follows the modal form. Taking the absolute value and normalizing the eigenfunction $\widetilde{u}_e$ by its maximum value along η we find

$$|\bar{u}_e(\hat{x},\eta)| = \mathtt{A}\;\frac{|\widetilde{u}_e(\eta)|}{|\widetilde{u}_e(\eta)|_{\max}}\; e^{\int_{\hat{x}_\mathrm{M}}^{\hat{x}} \sigma_{\mathrm{EV,\,Re}}(x)\mathrm{d}x}, \tag{3.2}$$

where $\mathtt{A}$ is undetermined because the eigenfunction is only obtained to within an undefined constant. If we only consider the maximum value along η, (3.2) simplifies to

$$|\bar{u}_e(\hat{x})|_{\max} = \mathtt{A}\; e^{\int_{\hat{x}_\mathrm{M}}^{\hat{x}} \sigma_{\mathrm{EV,\,Re}}(x)\mathrm{d}x}. \tag{3.3}$$

We then express the amplitude of the LUBR streamwise velocity $\bar{u}(\hat{x},\eta)$ in an analogous form,

$$|\bar{u}(\hat{x})|_{\max} = \mathtt{A}(\hat{x})\; e^{\int_{\hat{x}_\mathrm{M}}^{\hat{x}} \sigma_{\mathrm{EV,\,Re}}(x)\mathrm{d}x}, \tag{3.4}$$

which defines the streamwise-dependent receptivity coefficient $\mathtt{A}(\hat{x})$ implicitly. Equation (3.4) shows that from $\mathtt{A}(\hat{x})$ and the EV solution it is possible to obtain the LUBR maximum amplitude of the streamwise velocity perturbation inside the boundary layer and therefore investigate the influence of the outer disturbances in terms of k_y, $k_x\mathtt{R}$, and $\mathtt{G}$. We note that $\mathtt{A} = \mathtt{A}(\hat{x})$ is streamwise dependent. It would be constant only if the growth rate computed from the boundary region solution, $|\bar{u}'(\hat{x})|_{\max}/|\bar{u}(\hat{x})|_{\max}$, were equal to $\sigma_{\mathrm{EV,\,Re}}(\hat{x})$, i.e., the streamwise dependence of the LUBR solution were completely predicted by the EV growth rate. This is however not the case because the EV solution does not take into account the influence of the oncoming flow.

Figure 7 (left) shows the influence of $k_x\mathtt{R}$ and k_y on $\mathtt{A}(\hat{x})$, normalized by the values of $\mathtt{A}(\hat{x}_\mathrm{M})$ found in table 2. The boundary-layer perturbations are more influenced by the oncoming flow conditions as the frequency increases. The receptivity coefficient is nearly constant only for $k_x\mathtt{R} = 0$ and large $\hat{x}$. The intense effect of the frequency was also noted by Boiko *et al.* (2017) through a receptivity coefficient defined by optimal disturbances. As the frequency increases the effect of k_y increases as well. As $\mathtt{G}$ increases, the influence of k_y decreases and $\mathtt{A}(\hat{x})$ becomes more independent of $\hat{x}$, i.e., the solution $|\bar{u}(\hat{x})|_{\max}$ evolves closer to a pure exponential form in a wider $\hat{x}$-range. This is expected because the EV exponential solution (3.1) is valid in the asymptotic limit $\mathtt{G} \gg 1$.

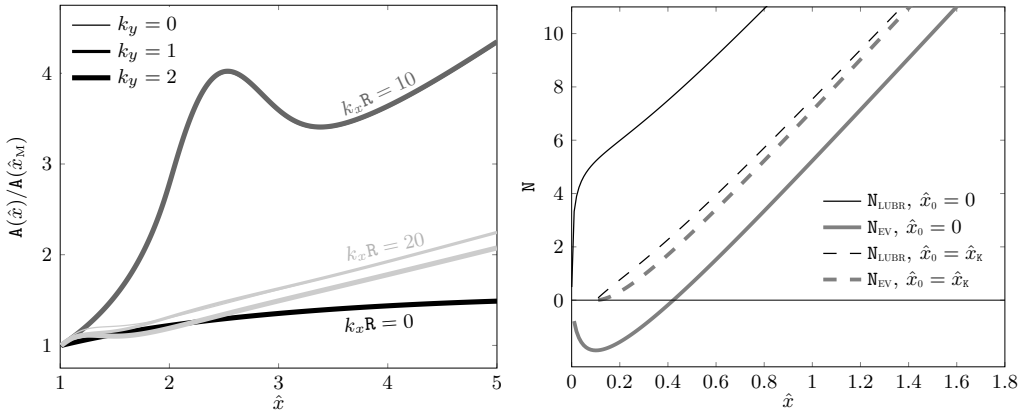

Figure 7: Influence of frequency $k_x\mathtt{R}$ and k_y on the normalized coefficient $\mathtt{A}(\hat{x})$ for $\mathtt{G} = 300$ (left). Amplification factor N based on the LUBR and EV approaches calculated at different starting locations for $k_x\mathtt{R} = 0$, $\mathtt{G} = 300$, $k_y = 1$ (right).

$k_x\mathtt{R}$	$k_y = 0$	$k_y = 1$	$k_y = 2$
0	66.60	60.56	47.48
10	13.51	15.40	14.06
20	0.31	0.44	0.54

Table 2: Receptivity coefficient $\mathtt{A}(\hat{x}_\mathrm{M})$ for $\mathtt{G} = 300$.

3.4. N-*factor*

We close this paper with a comment on the effect of free-stream disturbance on the amplification factor (or N-factor) widely used in transition-prediction studies (Van Ingen 1956; Jaffe *et al.* 1970) and defined as

$$\mathtt{N}(\hat{x}) \equiv \int_{\hat{x}_0}^{\hat{x}} \sigma(x)\mathrm{d}x, \tag{3.5}$$

where σ is the growth rate computed through either the LUBR or the EV solution, leading to $\mathtt{N}_{\mathrm{LUBR}}$ and $\mathtt{N}_{\mathrm{EV}}$, respectively. Engineers have used the value $\mathtt{N} = 9$ to predict the streamwise location where transition occurs, but, as figure 7 (right) shows, this approach is ambiguous. Not only does the N-factor calculated through the EV solution significantly underestimate the N-factor at fixed $\hat{x}$ computed through the LUBR solution, but there is also a strong dependence on the starting location where the N-factor is computed. The disagreement between $\mathtt{N}_{\mathrm{LUBR}}$ and $\mathtt{N}_{\mathrm{EV}}$ increases significantly when the N-factor is computed from $\hat{x}_0 = 0$. This is due to the rapid initial growth of K-vortices which the simplified EV approach is unable to capture. The agreement between these two solutions improves if the N-factor is computed from $\hat{x}_0 = \hat{x}_\mathrm{K}$ (the location where the Görtler vortices start amplifying) or if $\hat{x}_0$ is in the region of modal growth. However, the definition of $\hat{x}_0$ still remains arbitrary and one has to carefully verify the conditions associated with the calculation of the N-factor when using it for transition prediction. The rigorous mathematical formulation of the Görtler flow based on the receptivity due to free-stream disturbances does not help improve the reliability of the N-factor approach

for the transition prediction, in line with previous works revealing problems with this methodology (Smith 1955; Malik *et al.* 1999; Boiko *et al.* 2017).

Our work on the neutral curve can be further generalized by taking into account the influence of convex curvature and by introducing the nonlinear effects studied by Xu *et al.* (2017), therefore relaxing the assumption of small-amplitude perturbations (Ustinov 2013).

We wish to acknowledge the support of the US Air Force through the AFOSR grant FA9550-15-1-0248. We would also like to thank Dr M.E. Goldstein, Professor A.V. Boiko and Drs E. Marensi, P.D. Hicks, C. Alvarenga, and E. Zincone for providing insightful comments on a preliminary version of the paper. We also thank the referees for their useful comments.

REFERENCES

Bassom, A.P. & Seddougui, S.O. 1995 Receptivity mechanisms for Görtler vortex modes. *Theor. Comp. Fluid Dyn.* **7** (5), 317–339.

Boiko, A.V., Ivanov, A.V., Kachanov, Y.S. & Mischenko, D.A. 2010 Steady and unsteady Görtler boundary-layer instability on concave wall. *Europ. J. Mech. B/Fluids* **29** (2), 61–83.

Boiko, A.V., Ivanov, A.V., Kachanov, Y.S., Mischenko, D.A. & Nechepurenko, Y.M. 2017 Excitation of unsteady Görtler vortices by localized surface nonuniformities. *Theor. Comput. Fluid Dyn.* **31** (1), 67–88.

Goldstein, M.E. 1983 The evolution of Tollmien-Schlichting waves near a leading edge. *J. Fluid Mech.* **127**, 59–81.

Görtler, H. 1940 Uber eine Dreidimensionale Instabilitat Laminarer Grenzschichten am Konkaven Wanden. *Naschr Wiss Gas, Gottingen Math Phys Klasse* **2** (1).

Hall, P. 1982 Taylor-Görtler vortices in fully developed or boundary-layer flows: linear theory. *J. Fluid Mech.* **124**, 475–494.

Hall, P. 1983 The linear development of Görtler vortices in growing boundary layers. *J. Fluid Mech.* **130**, 41–58.

Hall, P. 1990 Görtler vortices in growing boundary layers: the leading edge receptivity problem, linear growth and the nonlinear breakdown stage. *Mathematika* **37** (74), 151–189.

Jaffe, N.A., Okamura, T.T. & Smith, A.M.O. 1970 Determination of spatial amplification factors and their application to predicting transition. *AIAA paper* **8** (2), 301–308.

Leib, S.J., Wundrow, D.W. & Goldstein, M.E. 1999 Effect of free-stream turbulence and other vortical disturbances on a laminar boundary layer. *J. Fluid Mech.* **380**, 169–203.

Malik, M.R., Li, F., Choudhari, M.M. & Chang, C. 1999 Secondary instability of crossflow vortices and swept-wing boundary layer transition. *J. Fluid Mech.* **399**, 85–115.

Ricco, P. 2009 The pre-transitional Klebanoff modes and other boundary layer disturbances induced by small-wavelength free-stream vorticity. *J. Fluid Mech.* **638**, 267–303.

Ricco, P. & Wu, X. 2007 Response of a compressible laminar boundary layer to free-stream vortical disturbances. *J. Fluid Mech.* **587**, 97–138.

Sescu, A. & Thompson, D. 2015 On the excitation of Görtler vortices by distributed roughness elements. *Theor. Comp. Fluid Dyn.* **29** (1-2), 67–92.

Smith, A.M.O. 1955 On the growth of Taylor-Görtler vortices along highly concave walls. *Quart. J. Math.* **13** (3), 233–262.

Squire, H.B. 1933 On the stability for three-dimensional disturbances of viscous fluid flow between parallel walls. In *Proc. R. Soc. Lond. A*, , vol. 142, pp. 621–628. The Royal Society.

Tollmien, W. 1929 Uber die Entstehung der Turbulenz 1. Mitteilung. in Math. Phys. Kl. (pp. 21–44). Nach. Ges. Wiss. Göttingen (Translated into English as NACA TM 609 (1931)) .

Ustinov, M.V. 2013 Boundary layer receptivity to the nonlinearly developing freestream turbulence. *Fluid Dynamics* **48** (5), 621–635.

Van Ingen, J.L. 1956 A suggested semi-empirical method for the calculation of the boundary

layer transition region. *Technische Hogeschool Delft, Vliegtuigbouwkunde, Rapport VTH-74* .

Wu, X., Zhao, D. & Luo, J. 2011 Excitation of steady and unsteady Görtler vortices by free-stream vortical disturbances. *J. Fluid Mech.* **682**, 66–100.

Xu, D., Zhang, Y. & Wu, X. 2017 Nonlinear evolution and secondary instability of steady and unsteady Görtler vortices induced by free-stream vortical disturbances. *J. Fluid Mech.* **829**, 681–730.